This article has been accepted for publication in a future issue of this journal, but has not been fully edited. Content may change prior to final publication. Citation information: DOI 10.1109/TIE.2017.2750614, IEEE Transactions on Industrial Electronics

Resonant current controller with enhanced transient response for grid-tied inverters

Claudio A. Busada, Sebastian Gomez Jorge and Jorge A. Solsona, *Senior Member, IEEE*

***Abstract*—This article highlights the limitations of the dynamic response of a grid-tied inverter connected through an inductor L when it is controlled using a proportional+resonant (PR) controller. Then, a new resonant current controller structure is proposed. This structure can be used to control the current injected by a grid-tied inverter through an L filter. When compared to the classic design, the proposed controller has better transient response, both to current reference and grid voltage changes. This is verified through simulation and experimental results.**

***Index Terms*—Current control, grid-tied inverters, PR controller**

I. Introduction

In general, the injection of energy to the grid from renewable resources is done via an inverter connected to it through passive filters [1]–[3]. These filters are used for filtering the ripple generated by the inverter. Many times the filter consists of an inductor. Controlling the current in the inductor is an extremely important topic in the injection process. The control algorithm should provide steady-state currents that have the lowest total harmonic distortion (THD) possible, according to recommendations in this regard [4]. In addition, it must have a good dynamic response, allowing compliance with response times imposed by the increasingly demanding grid codes [5], [6].

There are several linear current control strategies, which can be implemented in a synchronous reference frame [7], or in a stationary reference frame [8]. Within the latter category, the most popular are repetitive and resonant controllers [9], [10], controllers based on the internal model principle [11], and dead-beat controllers [12]. Resonant controllers can have a single resonance at the fundamental frequency of the grid, called proportional + resonant controller (PR) [13], or multiple resonances (PR + H). When the grid voltage does not contain harmonic frequency components a PR controller (applied to an ideal inverter), allows tracking of a fundamental frequency reference current with zero steady-state error. On the other hand, the PR + H controller ensures, in addition to the fundamental tracking, the rejection of the harmonic components for which it is tuned [14]–[17]. The PR controller is one of the most used in practice, because it generally provides an acceptable dynamic response, a current with low harmonic content, and avoids the use of coordinate transformations to a synchronous rotating frame. In [18], [19] a PR controller is compared to other commonly used current controllers.

Modern grid codes dictate that grid-tied inverters inject a specific amount of reactive current, within a maximum period of time, when a fault occurs in the grid [5], [6]. Such requirement makes it important to enhance the PR response or even yet to develop PR controllers with optimal transient response [20]. In presence of disturbances in the grid voltage (voltage sags or swells), the current controller must be able to quickly reject them, in order to track the current reference within the maximum stipulated period of time. Therefore, it is important to analyze and improve the dynamic response of the current controller, both to changes in the current reference and disturbances in the grid voltage [21], [22]. A method called active resistance is proposed in [23], which improves the bandwidth of disturbance rejection so that it results the same as the closed-loop current controller bandwidth.

In this article, the optimally designed PR controller (ODPRC) [24], [25], is analyzed. Given a desired phase margin, the optimum design provides the largest possible gains for the controller, taking into account factors such as the transport and sampling delays associated with the control calculation, and modulation processes. It is known that maximizing the gains does not necessarily imply achieving the best possible time-domain response [26]. Limitations on time-domain response to both changes in the current reference and to disturbances in the grid, are highlighted in the present article. In order to overcome these limitations, a new resonant controller structure is proposed. The controller places closed loop poles in arbitrary positions. Unlike other strategies which exclusively emphasize the location of the closed loop poles of the system [27], [28], the proposed controller ensures the cancelation of the closed loop zeros. This cancelation ensures an excellent temporal response when the reference current is changed. The proposal in [23] also ensures an excellent temporal response when the reference current is changed (first order response). However, [23] only allows to place the closed loop poles on a bounded region over the stable real axis, in a continuos time implementation, while the proposed controller allows to place them at arbitrary positions in a digital implementation (where the system's order is increased due to the processing delay). Simulation and experimental results are presented to show the advantages of the proposed controller.

This work was partially supported by Universidad Nacional del Sur, CONICET and ANPCyT, Argentina.

Claudio A. Busada, Sebastian Gomez Jorge and Jorge A. Solsona are with the Instituto de Investigaciones en Ingeniería Eléctrica (IIIE), Universidad Nacional del Sur (UNS)-CONICET and Dpto. Ing. Eléctrica y de Computadoras, UNS, Av. Alem 1253, (8000) Bahía Blanca, Argentina. (e-mail: cbusada@uns.edu.ar; sebastian.gomezjorge@uns.edu.ar; jsolsona@uns.edu.ar).

This article has been accepted for publication in a future issue of this journal, but has not been fully edited. Content may change prior to final publication. Citation information: DOI 10.1109/TIE.2017.2750614, IEEE Transactions on Industrial Electronics

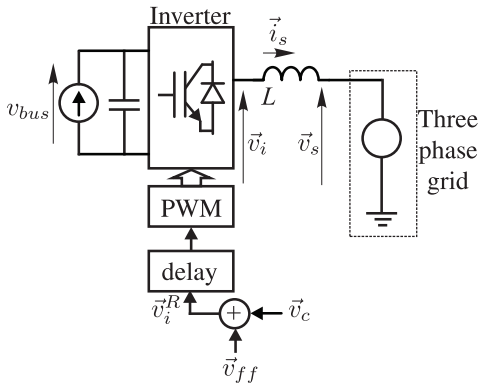

Fig. 1: System under study.

II. Classic PR controller

Figure 1 shows a three-phase grid-tied inverter, connected via an inductor L. Variables are denoted using complex vector notation, and are referred to an $\alpha\beta$ stationary reference frame. Variables $\vec{v}_i = v_{i\alpha} + jv_{i\beta}$ and $\vec{v}_s = v_{s\alpha} + jv_{s\beta}$ represent the output voltage of the inverter and the grid voltage, respectively. The behavior of the inductor current is described by:

$$Ld\vec{i_s}/dt = \vec{v}_i - \vec{v}_s, \tag{1}$$

where $\vec{i}_s = i_{s\alpha} + ji_{s\beta}$ is the inductor current. In Fig. 1, $\vec{v}_i^R$ represents the voltage reference imposed to the PWM modulator. This voltage is the sum of $\vec{v}_{ff}$ plus $\vec{v}_c$, where $\vec{v}_{ff}$ is a feedforward voltage used to cancel the effect of $\vec{v}_s$ on $\vec{i}_s$, and $\vec{v}_c$ is the voltage supplied by the current controller. It is assumed that there is a one-sample delay between $\vec{v}_i^R$ and $\vec{v}_i$, to model the delay introduced by a digital signal processor (DSP) in a practical implementation. In order to model the behavior of the current $\vec{i_s}$ in discrete time, (1) must be discretized with a sampling time T_s. This discretization results:

$$\vec{i_s}(k+1) = \vec{i_s}(k) + \frac{T_s}{L}\left[\vec{v}_i(k) - \vec{v}_s(k)\right], \tag{2}$$

where $\vec{v}_s(k)$ is the mean value of $\vec{v}_s(t)$ in the interval $kT_s \leq t \leq (k+1)T_s$.

The processing delay in Fig. 1, results in $\vec{v}_i(k+1) = \vec{v}_i^R(k) = \vec{v}_{ff}(k) + \vec{v}_c(k)$. Replacing this in the previous equation it results:

$$\vec{i_s}(k+1) = \vec{i_s}(k) + \frac{T_s}{L}\left[\vec{v}_c(k-1) + \overbrace{\vec{v}_{ff}(k-1) - \vec{v}_s(k)}^{\vec{v}_p(k)}\right], \tag{3}$$

where the disturbance voltage

$$\vec{v}_p(k) = \vec{v}_{ff}(k-1) - \vec{v}_s(k), \tag{4}$$

was defined. Then, performing the z transform of (3), results:

$$\vec{I}_s(z) = \frac{T_s/L}{z(z-1)}\vec{V}_c(z) + \frac{T_s/L}{z-1}\vec{V}_p(z), \tag{5}$$

where variables in capitals denote the z transform of the corresponding lower case variable, and $\vec{V}_p$ is the z transform of the disturbance voltage. Equation (5) is represented by block "Plant" in Fig. 2. This block includes the effect of the PWM, by using the zero-order-hold discretization.

In what follows, the synthesis of $\vec{v}_c$ by a PR controller is analyzed. In discrete-time, the best discretization of the PR controller results [24]:

$$G_c(z) = \frac{\vec{V}_c(z)}{\vec{I}_s^R(z) - \vec{I}_s(z)} = K_p\left[1 + \frac{1}{T_r}\frac{a_s(z^2-1)}{z^2 + b_1 z + 1}\right], \tag{6}$$

where K_p and T_r are the proportional gain and the time constant of the controller, respectively, $a_s = \sin(\omega_g T_s)/(2\omega_g)$ and $b_1 = -2\cos(\omega_g T_s)$, where ω_g is the fundamental angular frequency of the grid voltage. Controller (6) has two poles, located at $z = e^{\pm j\omega_g T_s}$, that in continuous-time are mapped to $s = \pm j\omega_g$ (according to the transformation $s = \ln(z)/T_s$). Rearranging the terms in (6):

$$G_c(z) = K_p\frac{A_c(z)}{B_c(z)} = K_p\frac{a_2 z^2 + a_1 z + a_0}{z^2 + b_1 z + 1}, \tag{7}$$

where $a_2 = (1 + a_s/T_r)$, $a_1 = b_1$ and $a_0 = (1 - a_s/T_r)$. Figure 2(a) shows the PR controller scheme. The ODPRC is obtained by choosing K_p and T_r, according to the following expressions [24], [25]:

$$K_p = \frac{\pi L}{6T_s}, \qquad T_r = \frac{60T_s}{\pi}. \tag{8}$$

With these values of K_p and T_r, the phase margin of the open loop transfer function is approximately $45°$, and the cross frequency $f_c = 1/(12T_s)$. For the closed loop system, from (5)-(8) it results:

$$\begin{aligned}\vec{I}_s(z) &= \overbrace{\frac{\frac{\pi}{6}A_c(z)}{z(z-1)B_c(z) + \frac{\pi}{6}A_c(z)}}^{G_i(z)}\vec{I}_s^R(z) \\ &+ \frac{T_s}{L}\overbrace{\frac{zB_c(z)}{z(z-1)B_c(z) + \frac{\pi}{6}A_c(z)}}^{G_v(z)}\vec{V}_p(z).\end{aligned} \tag{9}$$

In (9) transfer functions $G_i(z)$ and $G_v(z)$ are defined. Note that transfer functions $G_i(z)$ and $G_v(z)$ do not depend on L. This indicates that the analysis performed below is general, valid for any controller designed using (8), independent of the value of L.

In what follows it will be assumed that L =3.78mH, the sampling frequency $1/T_s = 10$kHz and that the fundamental frequency of the grid voltage is 50Hz.

A. $G_i(z)$ analysis

Transfer function $G_i(z)$ in (9) can be written as:

$$G_i(z) = \frac{\pi a_2}{6}\frac{(z - z_L)(z - z_L^*)}{(z - p_L)(z - p_L^*)(z - p_H)(z - p_H^*)}. \tag{10}$$

Here, superscript * represents the complex conjugate of the variable. This transfer function has two zeros, $z_L = 0.974\angle 0.994°$ and z_L^*, and four poles, $p_L = 0.971\angle 0.9084°$, p_L^*, $p_H = 0.735\angle 44.057°$ and p_H^*. Figure 3(a) shows the location of both zeros and poles of $G_i(z)$ in the z plane. Poles p_L and p_L^* have the largest modules (slower dynamic response). These are mapped to $s = -0.92\omega_g \pm j0.5\omega_g$ in

This article has been accepted for publication in a future issue of this journal, but has not been fully edited. Content may change prior to final publication. Citation information: DOI 10.1109/TIE.2017.2750614, IEEE Transactions on Industrial Electronics

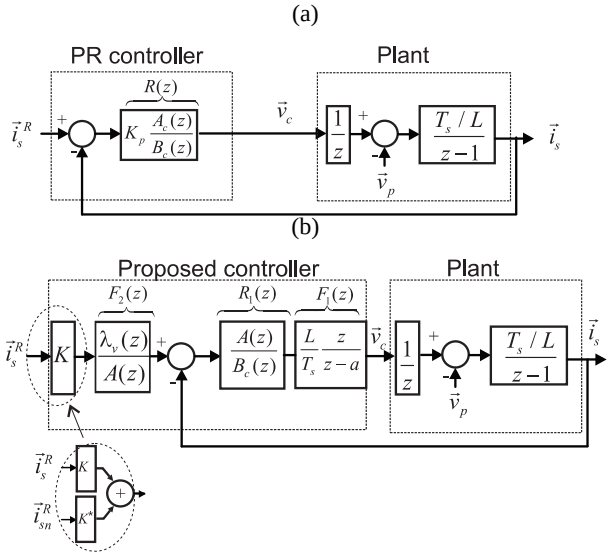

Fig. 2: (a) PR controller. (b) Proposed controller.

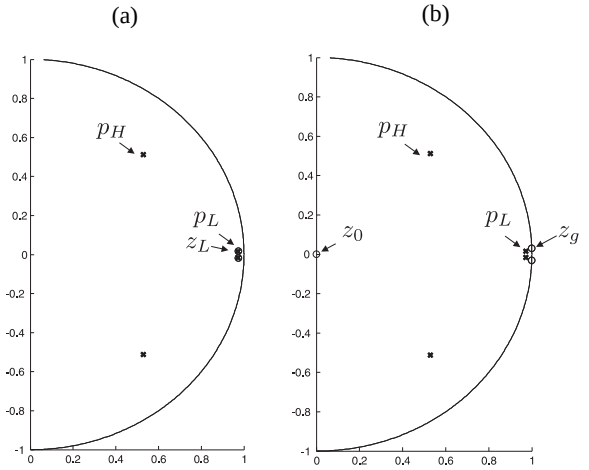

Fig. 3: Zeros and poles location in the z plane: (a) of $G_i(z)$; (b) of $G_v(z)$.

Laplace's plane. In a second order system, these poles indicate a time response with a settling time to 2% of the final value equal to $T_{set} = 4/(0.92\omega_g) = 13.7$ms. However, with the PR controller designed according to (8), the current settling time is much smaller than 13.7ms. This is due to the proximity between zeros $z_L = 0.974\angle 0.994°$ and z_L^*, and poles $p_L = 0.971\angle 0.9084°$ and p_L^*, mostly cancels the effect of these poles in the time response. This cancelation makes the time response dependent mainly on poles $p_H = 0.735\angle 44.057°$ and p_H^* of (10), which are located closer to the origin in the z plane. These are mapped to $s = -9.792\omega_g \pm j24.47\omega_g$ in Laplace's s plane. Note from this mapping that these poles are not optimally damped (the real part must be equal to the imaginary part for optimal damping). The damping factor ζ of these poles is $\zeta = 0.37$, which corresponds to an overshoot close to 40% and a settling time $T_{set} = 4/(9.792\omega_g) = 1.3$ms.

Figure 4(a) shows the time response of $|\vec{i}_s|$, for the discrete-time average value model of the system, defined in (9), when $\vec{v}_p$ and $\vec{i}_s^R$ start from zero at t<0, and a unitary positive sequence vector with angular frequency ω_g is suddenly applied to $\vec{i}_s^R$ at t=0. Note the presence of the initial transient, dominated by poles p_H and p_H^*. As expected, this transient has an overshoot close to 40%. Therefore, it is concluded that to operate safely at rated current levels, the converter must be designed to withstand an over-current of that magnitude. The settling time to 2% of the final value of the current in the figure is approximately 2.8ms (28 samples).

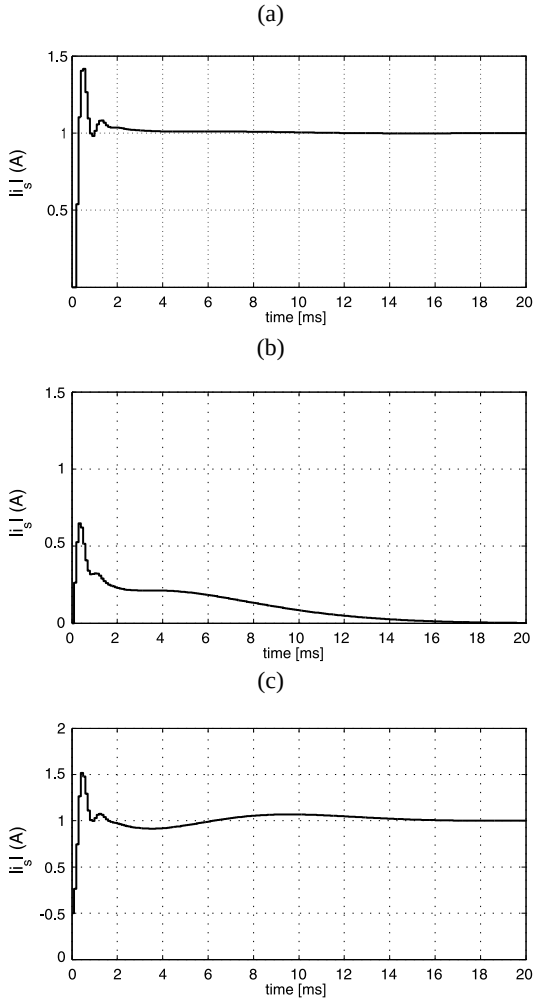

Fig. 4: PR controller. Time response of $|\vec{i}_s|$ for the discrete-time average value model of the system defined in (9), to the following inputs: (a) a step in $\vec{i}_s^R$; (b) a step in $\vec{v}_p$; (c) a step in both $\vec{i}_s^R$ and $\vec{v}_p$.

B. $G_v(z)$ analysis

Transfer function $G_v(z)$ defined in (9) has the same poles as $G_i(z)$, but different zeros: a zero z_0 at the origin, and two zeros on the unitary circle, located at $z_g = 1\angle 1.8°$ and z_g^* (at the roots of $B_c(z)$). These zeros are mapped to $s = \pm j\omega_g$. Figure 3(b) shows the location of zeros and poles of $G_v(z)$. Poles p_L and p_L^* of $G_v(z)$ do not have zeros as close to them as happens in $G_i(z)$. Therefore, the effect of these poles is noticeable in the dynamic response of $G_v(z)$.

This article has been accepted for publication in a future issue of this journal, but has not been fully edited. Content may change prior to final publication. Citation information: DOI 10.1109/TIE.2017.2750614, IEEE Transactions on Industrial Electronics

To verify this, Fig. 4(b) shows the time response of $|\vec{i}_s|$, for the discrete time average value model of the system, defined in (9). The response is obtained when $\vec{v}_p$ and $\vec{i}_s^R$ start from zero at t<0, and a positive sequence vector with angular frequency ω_g and magnitude 10V is suddenly applied to $\vec{v}_p$ at t=0. The response shows a high frequency oscillation which quickly extinguishes (due to the presence of poles p_H and p_H^*), mounted on a oscillation that extinguishes slowly. This last oscillation is originated by poles p_L and p_L^*, whose effect is no longer canceled by close zeros as in $G_i(z)$. Figure 4(c) shows the controller response when the current reference is the same as in Fig. 4(a), and there is a perturbation as the one used in Fig. 4(b). Unlike what happened in Fig. 4(a), the response time in which the current reaches 2% of the final value is now 15ms.

As can be seen, the dynamic response of the PR controller is impaired when in presence of disturbance $\vec{v}_p$ (see (4)). This is a clear disadvantage of the PR controller, since grid codes define the injection of specific reactive current values within a short time during grid fault conditions. It is therefore desirable to have a current controller with fast dynamic response when in presence of disturbances $\vec{v}_p$.

III. Proposed controller

Figure 2(b) shows the block diagram of the proposed controller, which, as the PR controller, is implemented in the $\alpha\beta$ stationary reference frame. Here, $a \in R$ and $K \in C$ are constants, $A(z)$ and $\lambda_v(z)$ are stable polynomials of the form $A(z) = a_2'z^2 + a_1'z + a_0'$ and $\lambda_v(z) = z^2 + \lambda_1 z + \lambda_0$, and $B_c(z) = z^2 + b_1 z + 1$ is the same monic polynomial used in PR controller (7) with $b_1 = -2\cos(\omega_g T_s)$. Comparing the proposed controller shown in Fig. 2(b) with the PR controller in Fig. 2(a), the following is concluded: a) Both controllers have the resonant section at the output of the error detector [block $R_1(z) = A(z)/B_c(z)$ in Fig. 2(b) and $R(z) = A_c(z)/B_c(z)$ in Fig. 2(a)]. Such resonant sections are of second order and zero relative degree. b) The proposed controller has an additional filter $F_1(z)$, which filters the control action. c) The proposed controller has a second filter $F_2(z)$, which filters the output current reference. This filtered reference is input to the error detector.

The closed loop system of Fig 2(b) is described by:

$$\vec{I}_s(z) = \frac{K\lambda_v(z)}{(z-a)(z-1)B_c(z) + A(z)}\vec{I}_s^R(z) + \frac{T_s}{L}\frac{B_c(z)(z-a)}{(z-a)(z-1)B_c(z) + A(z)}\vec{V}_p(z). \quad (11)$$

As can be seen in (11), the denominator of the closed loop transfer functions (of fourth order) depends only on the choice of constant a and polynomial $A(z)$ (of second order), since $B_c(z)$ is already defined. Note also, that filter $F_2(z)$ in Fig. 2(b) is not involved in the closed loop stability of the system.

Appendix A shows a method to find constant $a \in R$ and polinomial $A(z) = a_2'z^2 + a_1'z + a_0'$, so that the denominator of (11) is equal to any specified arbitrary polinomial $\lambda(z)$ of fourth order:

$$\lambda(z) = (z-a)(z-1)B_c(z) + A(z). \quad (12)$$

In particular, choosing this polinomial as:

$$\lambda(z) = \lambda_v(z)\lambda_i(z), \quad (13)$$

where $\lambda_i(z) = z^2 + \lambda_1' z + \lambda_0'$ is a stable polinomial, and $\lambda_v(z) = z^2 + \lambda_1 z + \lambda_0$ is the numerator polinomial of filter $F_2(z)$ [used to filter the current reference in Fig. 2(b)], the closed loop system (11) results:

$$\vec{I}_s(z) = \overbrace{\frac{K}{\lambda_i(z)}}^{G_{i1}(z)}\vec{I}_s^R(z) + \frac{T_s}{L}\overbrace{\frac{B_c(z)}{\lambda_i(z)}\frac{(z-a)}{\lambda_v(z)}}^{G_{v1}(z)}\vec{V}_p(z). \quad (14)$$

It is verified that transfer function $G_{i1}(z)$ between $\vec{i}_s^R$ and $\vec{i}_s$, defined in (14), has relative degree two, with no zeros. The zero-pole cancelation in the closed loop system makes the apparent order of the system, between output $\vec{i}_s$ and reference $\vec{i}_s^R$ the same as the order of plant (5), between $\vec{i}_s$ and $\vec{v}_c$. This feature is typical of P type linear controllers, and dead-beat controllers.

To ensure that in steady-state the controller can track a positive sequence current reference $\vec{i}_s^R$ of frequency ω_g without error, transfer function $G_{i1}(z)$ in (14) must fulfill $G_{i1}(e^{j\omega_g T_s}) = 1\angle 0^\circ$ (so that $\vec{i}_s$ has the same magnitude and phase as $\vec{i}_s^R$). This is accomplished if K [the gain used at the input of the filter $F_2(z)$ of Fig. 2(b)] is set equal to:

$$K = \lambda_i(z)|_{z=e^{j\omega_g T_s}}. \quad (15)$$

To summarize the design procedure: the controller designer only requires to properly choose polynomials $\lambda_v(z)$ and $\lambda_i(z)$, defined in (13) (thus choosing the resulting closed loop poles). Once that is done, gain K is obtained through (15), while constant a and polynomial $A(z)$ are chosen, as explained in Appendix A, so that closed loop polinomial (12) is equal to (13).

Note 1. During power grid failures it is usually necessary to inject some amount of negative sequence current. In this case, a negative sequence current reference $\vec{i}_{sn}^R$ should be added as a second input to the controller, as shown at the bottom of Fig. 2(b). In order for the injected current to copy this reference $\vec{i}_{sn}^R$ without error, a gain $K^* = \lambda_i(e^{-j\omega_g T_s})$ must be used. This gain is the conjugate complex of gain K used for reference $\vec{i}_s^R$.

A. Choosing $\lambda_i(z)$ and $\lambda_v(z)$.

Polynomial $\lambda_i(z) = z^2 + \lambda_1' z + \lambda_0'$ in (13) is chosen by the designer to obtain a fast transient response in $\vec{i}_s$ to a change in $\vec{i}_s^R$. Indeed, this polynomial determines transfer function $G_{i1}(z)$ defined in (14). To obtain a fast transient response, the following must be satisfied: $|roots\{\lambda_i(z)\}| \ll 1$. One possibility is to set $\lambda_1' = \lambda_0' = 0$, which locates both poles at the origin. This results in a dead-beat type controller, where $\vec{i}_s$ tracks a reference $\vec{i}_s^R$ of fundamental frequency without steady-state error, in only two samples. This is the fastest transient response that can be expected from a second-order system, as is plant (5). Due the fact that the proposed controller is a resonant controller, it has infinite rejection to perturbations of fundamental grid frequency. This is an advantage when compared to the standard dead beat controller

This article has been accepted for publication in a future issue of this journal, but has not been fully edited. Content may change prior to final publication. Citation information: DOI 10.1109/TIE.2017.2750614, IEEE Transactions on Industrial Electronics

[12]. To achieve this fast response, the dead-beat controller requires large control actions and, when compared to a slower controller, reduces the robustness of the system to mismatches in the value of inductor L with respect to its nominal value.

Another possible choice for $\lambda_i(z)$ is placing its poles over the real axis (to avoid overshoot) and close to the origin, at $z = e^{-\sigma_1 \omega_g T_s}$ and $z = e^{-\sigma_2 \omega_g T_s}$, with $\sigma_1, \sigma_2 \gg 1$. This leads to a transient response similar to that of the dead-beat controller (both controllers have fast transient response with no overshoot), but with smaller control actions, reducing the chances of saturating the PWM modulator (because the controller has more time to make the same desired current jump).

Figure 5(a) shows $|\vec{i}_s|$, for the discrete-time average value model of the system defined in (14)-(15), when $\vec{v}_p$ and $\vec{i}_s^R$ start from zero at t<0, and a positive sequence unitary vector of angular frequency ω_g is suddenly applied to $\vec{i}_s^R$ at t=0, for $\sigma_1 = 30$ and $\sigma_2 = 50$. Note that the overshoot seen in Fig. 4(a) is no longer present here, and the settling time to 2% of the final value is 0.6ms (6 samples, instead of the two samples corresponding to the dead beat controller).

Polynomial $\lambda_v(z)$ is only present in transfer function $G_{v1}(z)$ defined in (14). Assuming that $\lambda_i(z)$ has already been chosen, $\lambda_v(z)$ should be chosen by the designer to achieve a fast transient response to reject grid voltage disturbances. Setting the roots of $\lambda_v(z)$ to $z = e^{(-1 \pm j)\sigma_v \omega_g T_s}$, with $\sigma_v \gg 1$ has shown good practical results. In the Laplace domain, these roots are mapped to $s = (-1 \pm j)\sigma_v \omega_g$ and result in an optimally damped response, with $\zeta = 0.707$.

Figure 5(b) shows $|\vec{i}_s|$, for system (14)-(15), when $\vec{v}_p$ and $\vec{i}_s^R$ start from zero at t<0, and a positive sequence vector of angular frequency ω_g and magnitude 10V is suddenly applied to $\vec{v}_p$ at t=0, for $\sigma_1 = 30$, $\sigma_2 = 50$ and $\sigma_v = 5$. Figure 5(c) shows the transient response of the controller when the current reference is the same as the one used in Fig. 5(a), and there is a disturbance as the one used in Fig. 5(b). The current response time to 2% of the final value is now 2.6ms, more than five times smaller than that shown in Fig. 4(c).

B. Stability of $A(z)$ and robustness

Polynomial $A(z)$ must be stable to be used as the denominator of the filter applied to $\vec{i}_s^R$ in Fig. 2(b). To verify its stability, σ_v, σ_1 and σ_2 were varied within proper bounds, and the root locus of $A(z)$ was computed for each combination of $\{\sigma_v, \sigma_1, \sigma_2\}$. The variation bounds were: $1 \leq \sigma_v \leq 50$, $10 \leq \sigma_1 \leq 100$ and $10 \leq \sigma_2 \leq 100$. These include the design values recommended in previous section. Figure 6a shows a plot of the resulting root locus, which verifies that $A(z)$ is a stable polynomial.

To verify the robustness of the controller against uncertainties in the value of L, Fig. 6(b) shows a detail of repeating the step response of Fig. 5(a), for deviations of $\pm 20\%$ in the value of L with respect to the nominal value used to tune the controller, L_{nom} =3.78mH. Note that the system preserves stability, and that the resulting overshoot (which is 9.8% for $L = 1.2 L_{nom}$), is lower than that observed in Fig. 4(a), corresponding to the ODPRC.

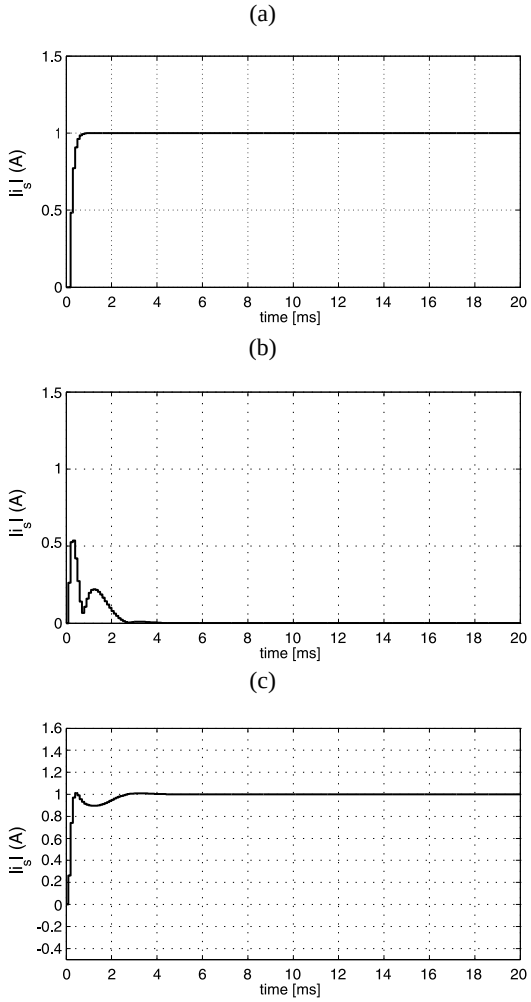

Fig. 5: Proposed controller. Time response of $|\vec{i}_s|$ for the discrete-time average value model of the system defined in (14)-(15), to the following inputs: (a) a step in $\vec{i}_s^R$; (b) a step in $\vec{v}_p$; (c) a step in both $\vec{i}_s^R$ and $\vec{v}_p$.

IV. Simulation results

A grid-tied inverter was simulated, with a bus voltage $V_{bus} = 400$ and 1μs of switch dead-time. The sampling frequency was set to 10kHz.The value of the connection inductor was $L = 3.78$mH with a series resistance $R = 0.5\Omega$. Also, the noise of the 12bit AD converters of the DSP used to obtain the experimental results was included in the simulation model. This noise was modeled through an uniformly distributed random signal, with a maximum magnitude of ± 6 counts. Grid voltage $\vec{v}_s$ used in the simulation was set to 110Vrms, with a THD of 3.1%.

Feedforward voltage $\vec{v}_{ff}(k)$ (see Fig. 1) is chosen proportional to measured grid voltage $\vec{v}_s(k)$. This means that $\vec{v}_{ff}(k) = K_v \vec{v}_s(k)$, where K_v is a constant. In this way, according to (4), the disturbance to which the system is subject results $\vec{v}_p(k) = K_v \vec{v}_s(k-1) - \vec{v}_s(k)$. Varying the value of K_v online makes it possible to evaluate the behavior of the system to variations in $\vec{v}_p$, without the need of a programmable grid voltage source.

This article has been accepted for publication in a future issue of this journal, but has not been fully edited. Content may change prior to final publication. Citation information: DOI 10.1109/TIE.2017.2750614, IEEE Transactions on Industrial Electronics

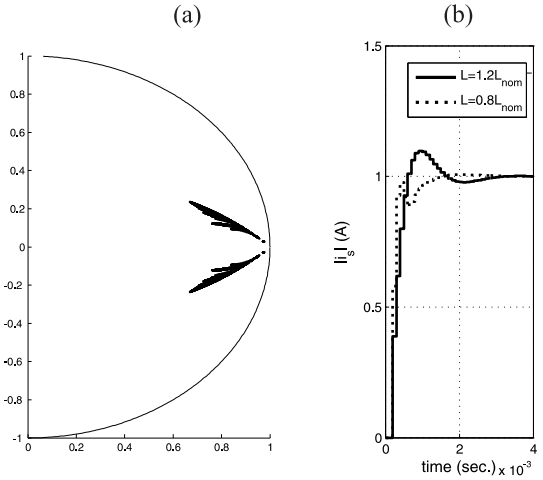

Fig. 6: (a) Root locus of $A(z)$ for $1 \leq \sigma_v \leq 50$, $10 \leq \sigma_1 \leq 100$ and $10 \leq \sigma_2 \leq 100$. b) Robustness to uncertainty in the value of L.

The PR controller was simulated, designed according to (8). Figure 7(a) shows the current injected by the PR controller in the three phases, I_{abc}, and the module of the current vector $|\vec{i}_s|$. With $K_v = 0$, at $t = 10$ms a step jump is performed in the magnitude of reference $\vec{i}_s^R$, from 0Apeak to 10Apeak. This reference is a positive sequence vector of angular frequency ω_g. The behavior of $|\vec{i}_s|$ to this event is shown at the bottom of the figure. As can be seen, the behavior is similar to that shown in Fig. 4(a). However, the overshoot here is 3.62A (36%). This overshoot is smaller than the theoretical one because of the winding resistance, which adds damping.

In another simulation, current reference $\vec{i}_s^R$ is kept at zero, and a disturbance $\vec{v}_p$ is introduced. At $t = 2$ms a step change from $K_v = 1$ to $K_v = 0.5$ is produced. The injected current, according to Fig. 7(b), takes approximately 15ms to converge to its steady-state value. This matches what was seen in Fig. 4(b). It is then verified that the dynamic response of the PR controller to disturbances is slow, compared to its response to changes in current reference $\vec{i}_s^R$.

Figure 7(c) shows the simulation results when both the current reference magnitude and K_v are varied as in the two previous simulations. As can be seen, the settling time is now 15ms, similar to that shown in Fig. 4(c)

Simulation results were also obtained using the proposed controller, designed with $\sigma_1 = 30$, $\sigma_2 = 50$ and $\sigma_v = 5$ (the same parameters used to plot Fig. 5). These results are shown in Fig. 8. It is verified in Fig. 8(a) that after the step magnitude change in $\vec{i}_s^R$ at $t = 10$ms, the current transient response is better than that of the PR controller, as predicted in Fig. 5(a). Additionally, Fig. 8(b) shows that after the magnitude step in $\vec{v}_p$ at $t = 2$ms, the proposed controller stabilizes the current in approximately 4ms, as predicted in Fig. 5(b). Figure 8(c) shows the simulation results when both the current reference magnitude and K_v are varied as in the two previous simulations. As can be seen, the settling time is now 4ms, similar to that shown in Fig. 5(c). It is verified that the transient response of the proposed controller is superior to that of the PR controller, both to changes in $\vec{i}_s^R$ as well as in $\vec{v}_p$.

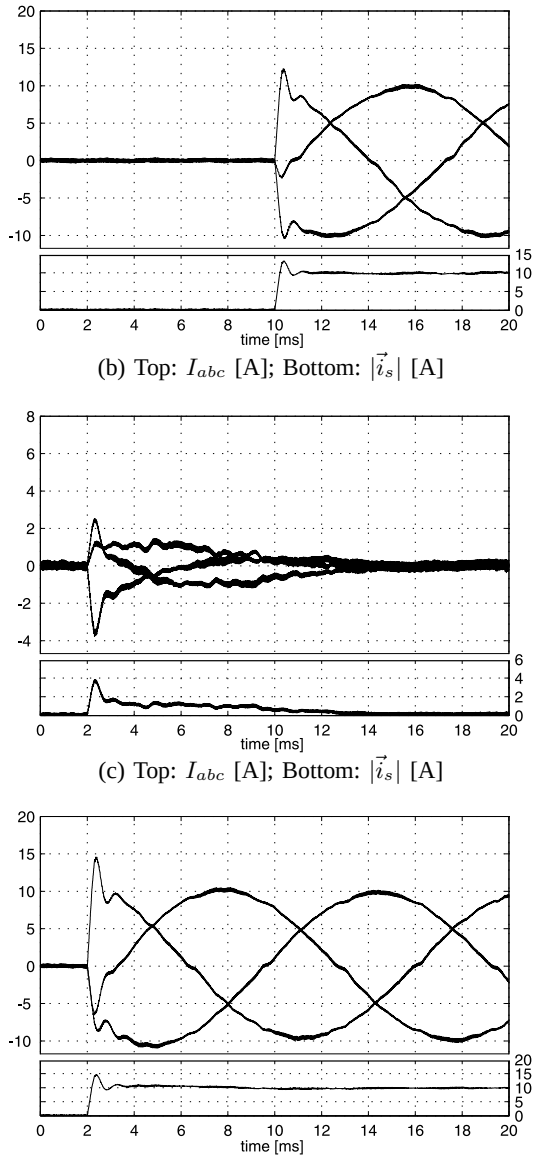

Fig. 7: Simulation results for the PR controller (time scale in [ms]). On all figures: top phase currents, bottom $|\vec{i}_s|$.(a) for a current reference magnitude step from 0 to 10Apeak (scale: 5A/div, 2ms/div). (b) with $\vec{i}_s^R = 0$ when a magnitude step in $\vec{v}_{ff}$ from $K_v = 1$ to $K_v = 0.5$ is performed (scale: 2A/div, 2ms/div): (c) both current reference step and K_v step at the same time (scale: 5A/div, 2ms/div).

V. Experimental results

A prototype of the simulated system was implemented for the experimental verification. A three-phase inverter was used, built using IRG4PH50UD IGBTs. Both controllers were implemented in a TMS320F28335 DSP, with a sampling frequency of 10kHz. Grid voltage $\vec{v}_s$ had a magnitude of 110Vrms and a THD of 3.1%.

Figure 9 and Fig. 10 show the experimental results obtained from the implementation of both the PR controller and the

This article has been accepted for publication in a future issue of this journal, but has not been fully edited. Content may change prior to final publication. Citation information: DOI 10.1109/TIE.2017.2750614, IEEE Transactions on Industrial Electronics

(a) Top: I_{abc} [A]; Bottom: $|\vec{i}_s|$ [A]

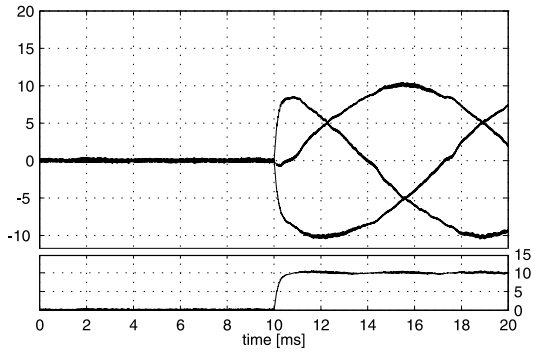

(b) Top: I_{abc} [A]; Bottom: $|\vec{i}_s|$ [A]

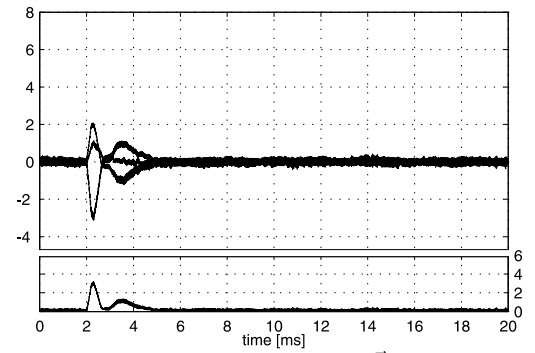

(c) Top: I_{abc} [A]; Bottom: $|\vec{i}_s|$ [A]

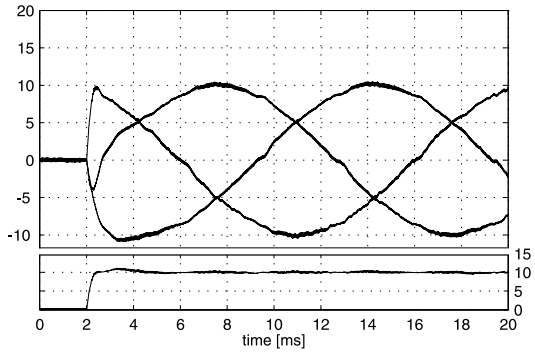

Fig. 8: Simulation results for the proposed controller (time scale in [ms]). On all figures: top phase currents, bottom $|\vec{i}_s|$.(a) for a current reference magnitude step from 0 to 10Apeak (scale: 5A/div, 2ms/div). (b) with $\vec{i}_s^R = 0$ when a magnitude step in $\vec{v}_{ff}$ from $K_v = 1$ to $K_v = 0.5$ is performed (scale: 2A/div, 2ms/div): (c) both current reference step and K_v step at the same time (scale: 5A/div, 2ms/div).

(a) Top: I_{abc} [A]; Bottom: $|\vec{i}_s|$ [A]

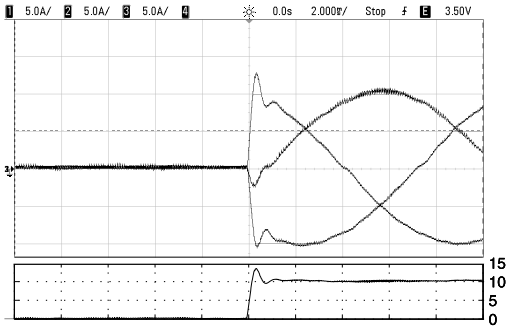

(b) Top: I_{abc} [A]; Bottom: $|\vec{i}_s|$ [A]

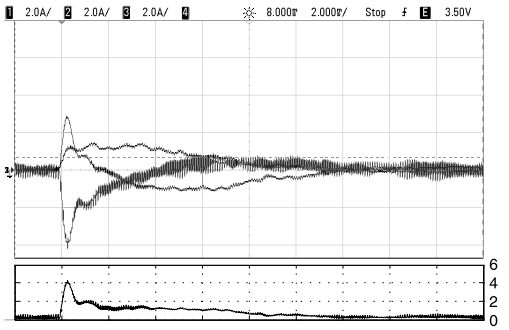

(c) Top: I_{abc} [A]; Bottom: $|\vec{i}_s|$ [A]

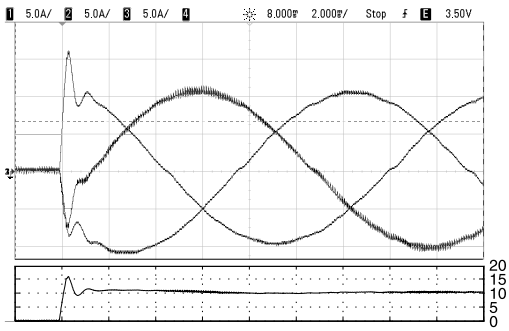

Fig. 9: Experimental results for the PR controller. On all figures: top phase currents, bottom $|\vec{i}_s|$.(a) for a current reference magnitude step from 10Apeak to 5Apeak (scale: 5A/div, 2ms/div). (b) with $\vec{i}_s^R = 0$ when a magnitude step in $\vec{v}_{ff}$ from $K_v = 1$ to $K_v = 0.7$ is performed (scale: 2A/div, 2ms/div): (c) both current reference step and K_v step at the same time (scale: 5A/div, 2ms/div).

proposed controller, respectively. These results are aimed to compare the dynamic responses of both controllers to variations in the current reference and to grid disturbances. Figure 9(a) shows the phase current injected by the PR controller. In this experiment the dynamic response of the controller is shown when a magnitude step from 0Apeak to 10Apeak is performed in current reference $\vec{i}_s^R$. Figure 10(a) shows the same results for the proposed controller. Looking at both figures it can be seen that the proposed controller has better transient response.

In order to test the disturbance rejection capabilities of both controllers, current reference $\vec{i}_s^R$ was set to zero and a voltage disturbance was produced varying $\vec{v}_{ff}$ through a step from $K_v = 1$ to $K_v = 0.5$. The results of this experiment for the PR controller are shown in Fig. 9(b), and for the proposed controller in Fig. 10(b). In these figures, the phase currents are shown. As can be seen, the proposed controller converges noticeably faster than the PR controller.

Finally, Fig. 9(c) and Fig. 10(c) show the response of both controllers to a step in both $|\vec{i}_s^R|$ and K_v. As can be seen the results are similar to those of the simulations.

This article has been accepted for publication in a future issue of this journal, but has not been fully edited. Content may change prior to final publication. Citation information: DOI 10.1109/TIE.2017.2750614, IEEE Transactions on Industrial Electronics

(a) Top: I_{abc} [A]; Bottom: $|\vec{i}_s|$ [A]

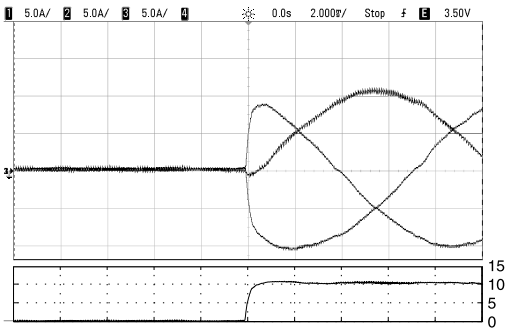

(b) Top: I_{abc} [A]; Bottom: $|\vec{i}_s|$ [A]

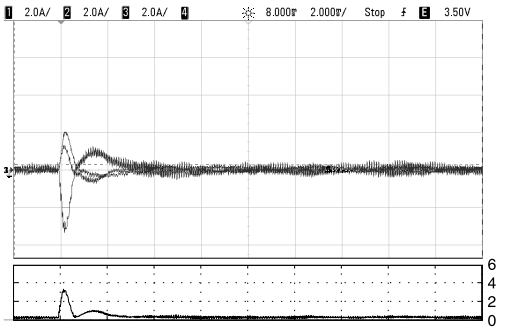

(c) Top: I_{abc} [A]; Bottom: $|\vec{i}_s|$ [A]

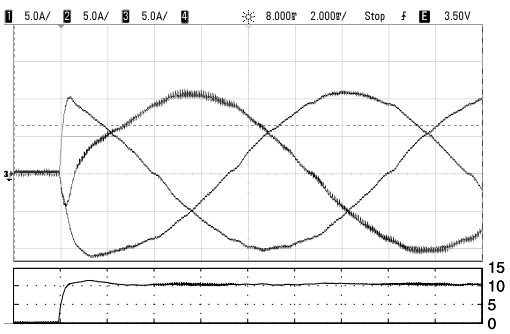

Fig. 10: Experimental results for the proposed controller. On all figures: top phase currents, bottom $|\vec{i}_s|$.(a) for a current reference magnitude step from 10Apeak to 5Apeak (scale: 5A/div, 2ms/div). (b) with $\vec{i}_s^R = 0$ when a magnitude step in $\vec{v}_{ff}$ from $K_v = 1$ to $K_v = 0.7$ is performed (scale: 2A/div, 2ms/div): (c) both current reference step and K_v step at the same time (scale: 5A/div, 2ms/div).

These results verify those obtained by simulation, showing that the proposed controller has better dynamic response to the PR controller designed according to (8).

Figure 11 shows experimental validation of the robustness test introduced for the theoretical system in Fig. 6(b). For these tests, the inductance used for the design of the controller, L_{nom}, was set to +25/-17% of the value actual system inductance L =3.78mH (this guarantees a variation of $L = \pm 20\% L_{nom}$) . As can be seen the results are very similar to the theoretical results shown in Fig. 6(b).

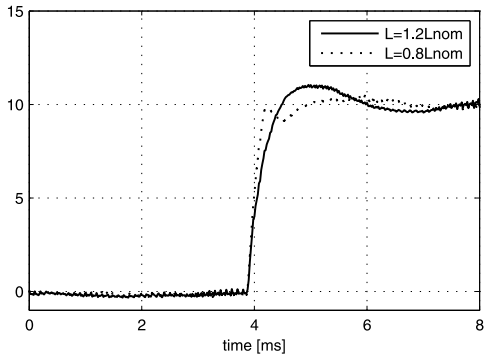

Fig. 11: Experimental robustness to uncertainty in the value of L_{nom}.

VI. Conclusions

Having highlighted the limitations of the ODPRC in the control of an inverter connected to the grid via an inductor, a current controller for a three-phase grid-tied inverter connected through an L filter was presented. The controller proposed here was compared to an ODPRC. The results show that the proposed controller has better dynamic response, both to changes in the current reference and to grid voltage disturbances. A design method for the new controller was proposed, which allows to arbitrarily locate the closed loop poles of the system. The results were validated through simulation and experimental results.

Appendix A

There is a polynomial $A(z)$ of degree two or less and a constant a, that make the denominator polinomial of (11) equal to any defined arbitrary polinomial $\lambda(z)$ of fourth degree. To verify this statement, let $\lambda(z) = z^4 + \lambda_3 z^3 + \lambda_2 z^2 + \lambda_1 z + \lambda_0$ be an arbitrary monic polynomial. Note that in the denominator of the transfer functions in (11), the term $(z-1)B_c(z)$ is a monic polynomial of third degree. The ratio between $\lambda(z)$ (monic of fourth degree) and $(z-1)B_c(z)$ (monic of third degree) is always of the form:

$$\frac{\lambda(z)}{(z-1)B_c(z)} = (z-a) + \frac{A(z)}{(z-1)B_c(z)}, \qquad (16)$$

where $z-a$ is the quotient, and $A(z)$, of degree two or less, is the reminder. The above equation implies that:

$$\lambda(z) = (z-a)(z-1)B_c(z) + A(z). \qquad (17)$$

As can be seen, the right hand side of this equation is the denominator of the transfer functions in (11). Therefore, there is a polynomial $A(z)$ and constant a that verify (11). These can be found simply by performing the ratio shown in the left hand side of (16).

References

[1] H. Komurcugil, N. Altin, S. Ozdemir, and I. Sefa, "Lyapunov-function and proportional-resonant-based control strategy for single-phase grid-connected vsi with lcl filter," *IEEE Transactions on Industrial Electronics*, vol. 63, no. 5, pp. 2838–2849, 2016.

This article has been accepted for publication in a future issue of this journal, but has not been fully edited. Content may change prior to final publication. Citation information: DOI 10.1109/TIE.2017.2750614, IEEE Transactions on Industrial Electronics

[2] G. C. Konstantopoulos, Q.-C. Zhong, and W.-L. Ming, "Pll-less nonlinear current-limiting controller for single-phase grid-tied inverters: Design, stability analysis, and operation under grid faults," *IEEE Transactions on Industrial Electronics*, vol. 63, no. 9, pp. 5582–5591, 2016.
[3] J. F. Ardashir, M. Sabahi, S. H. Hosseini, F. Blaabjerg, E. Babaei, and G. B. Gharehpetian, "A single-phase transformerless inverter with charge pump circuit concept for grid-tied pv applications," *IEEE Transactions on Industrial Electronics*, 2016.
[4] "IEEE standard for interconnecting distributed resources with electric power systems," *IEEE Std 1547-2003*, 2003.
[5] "Transmission code 2007. networks and system rules of the german transmission system operators," *VDN-e.v. beim VDEW*, Aug. 2007.
[6] "ENTSO-E network code for requirements for grid connection applicable to all generators," *European Network for Transmission System Operators for Electricity*, Jun. 2012.
[7] M. Reyes, P. Rodriguez, S. Vazquez, A. Luna, R. Teodorescu, and J. Carrasco, "Enhanced decoupled double synchronous reference frame current controller for unbalanced grid-voltage conditions," *Power Electronics, IEEE Trans. on*, vol. 27, no. 9, pp. 3934–3943, Sept 2012.
[8] D. Zmood and D. Holmes, "Stationary frame current regulation of pwm inverters with zero steady-state error," *Power Electronics, IEEE Trans. on*, vol. 18, no. 3, pp. 814–822, May 2003.
[9] W. Zhao, X. Ruan, D. Yang, X. Chen, and L. Jia, "Neutral point voltage ripple suppression for three-phase four-wire inverter with independently-controlled neutral module," *IEEE Transactions on Industrial Electronics*, 2016.
[10] A. Rodriguez, C. Giron, M. Rizo, V. Saez, E. Bueno, and F. Rodriguez, "Comparison of current controllers based on repetitive-based control and second order generalized integrators for active power filters," in *IECON '09*, Nov 2009, pp. 3223–3228.
[11] V. Blasko, L. Arnedo, P. Kshirsagar, and S. Dwari, "Control and elimination of sinusoidal harmonics in power electronics equipment: A system approach," in *ECCE, 2011 IEEE*, Sept 2011, pp. 2827–2837.
[12] J. Moreno, J. Huerta, R. Gil, and S. Gonzalez, "A robust predictive current control for three-phase grid-connected inverters," *Industrial Electronics, IEEE Trans. on*, vol. 56, no. 6, pp. 1993–2004, June 2009.
[13] D. Zmood, D. Holmes, and G. Bode, "Frequency-domain analysis of three-phase linear current regulators," *Ind. Appl., IEEE Trans. on*, vol. 37, no. 2, pp. 601–610, Mar 2001.
[14] M. Castilla, J. Miret, A. Camacho, J. Matas, and L. de Vicuna, "Reduction of current harmonic distortion in three-phase grid-connected photovoltaic inverters via resonant current control," *IEEE Transactions on Industrial Electronics*, vol. 60, no. 4, pp. 1464–1472, April 2013.
[15] X. Wang, F. Blaabjerg, M. Liserre, Z. Chen, J. He, and Y. Li, "An active damper for stabilizing power-electronics-based ac systems," *IEEE Transactions on Power Electronics*, vol. 29, no. 7, pp. 3318–3329, July 2014.
[16] J.-H. Lee, H.-G. Jeong, and K.-B. Lee, "Performance improvement of grid-connected inverter systems under unbalanced and distorted grid voltage by using a pr controller," *J Electr Eng Technol*, vol. 7, no. 6, pp. 918–925, 2012.
[17] A.Chatterjee and K. Mohanty, "Design and analysis of stationary frame pr current controller for performance improvement of grid tied pv inverters," in *Power Electronics (IICPE), 2014 IEEE 6th India International Conference on*, Dec 2014.
[18] A. Timbus, M. Liserre, R. Teodorescu, P. Rodriguez, and F. Blaabjerg, "Evaluation of current controllers for distributed power generation systems," *IEEE Transactions on Power Electronics*, vol. 24, no. 3, pp. 654–664, July 2009.
[19] T. Midtsund, J. Suul, and T. Undeland, "Evaluation of current controller performance and stability for voltage source converters connected to a weak grid," in *Power Electronics for Distributed Generation Systems (PEDG), 2010 2nd IEEE International Symposium on*, June 2010, pp. 382–388.
[20] A. Kuperman, "Proportional-resonant current controllers design based on desired transient performance," *Power Electronics, IEEE Transactions on*, vol. 30, no. 10, pp. 5341–5345, Oct 2015.
[21] A. Vidal, F. Freijedo, A. Yepes, P. Fernandez-Comesana, J. Malvar, O. Lopez, and J. Doval-Gandoy, "Assessment and optimization of the transient response of proportional-resonant current controllers for distributed power generation systems," *Industrial Electronics, IEEE Transactions on*, vol. 60, no. 4, pp. 1367–1383, April 2013.
[22] A. Vidal, F. Freijedo, A. Yepes, J. Malvar, O. Lopez, and J. Doval-Gandoy, "Transient response evaluation of stationary-frame resonant current controllers for grid-connected applications," *Power Electronics, IET*, vol. 7, no. 7, pp. 1714–1724, July 2014.
[23] A. Petersson, L. Harnefors, and T. Thiringer, "Evaluation of current control methods for wind turbines using doubly-fed induction machines," *IEEE Transactions on Power Electronics*, vol. 20, no. 1, pp. 227–235, Jan 2005.
[24] S. Parker, B. McGrath, and D. Holmes, "Regions of active damping control for lcl filters," *Ind. Appl., IEEE Trans. on*, vol. 50, no. 1, pp. 424–432, Jan 2014.
[25] D. Holmes, T. Lipo, B. McGrath, and W. Kong, "Optimized design of stationary frame three phase ac current regulators," *Power Electronics, IEEE Trans. on*, vol. 24, no. 11, pp. 2417–2426, Nov 2009.
[26] A. G. Yepes, A. Vidal, J. Malvar, O. Lopez, and J. Doval-Gandoy, "Tuning method aimed at optimized settling time and overshoot for synchronous proportional-integral current control in electric machines," *IEEE Transactions on Power Electronics*, vol. 29, no. 6, pp. 3041–3054, June 2014.
[27] C. A. Busada, S. G. Jorge, A. E. Leon, and J. A. Solsona, "Current controller based on reduced order generalized integrators for distributed generation systems," *IEEE Transactions on Industrial Electronics*, vol. 59, no. 7, pp. 2898–2909, July 2012.
[28] B. Li, W. Yao, L. Hang, and L. M. Tolbert, "Robust proportional resonant regulator for grid-connected voltage source inverter (vsi) using direct pole placement design method," *IET Power Electronics*, vol. 5, no. 8, pp. 1367–1373, September 2012.

Claudio A. Busada was born in Baha Blanca, Argentina, on March 13, 1962. He received the degree in electrical engineering from the Universidad Nacional del Sur, Baha Blanca, in 1989, and the Dr. degree in control systems in 2004, from the same University.

From 1988 to 2004, he was with the Mechanic and Electrical Department, City of Baha Blanca. Since 1989, he has been with the Departamento de Ingeniera Elctrica y de Computadoras (DIEC), Universidad Nacional del Sur, where he is a Professor. He is a Researcher of the the Instituto de Investigaciones en Ingeniera Elctrica "Alfredo C. Desages" (UNS-CONICET). His research interests include power electronics, rotating machinery, active filters, automatic control, and integration of distributed energy systems.

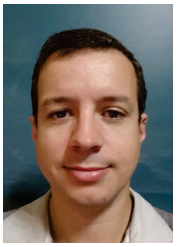

Sebastian Gomez Jorge received the Electronics Engineer, M.S., and Dr. degrees from the Universidad Nacional del Sur, Baha Blanca, Argentina, in 2006, 2009, and 2011, respectively.

He is currently with with CONICET at the Instituto de Investigaciones en Ingeniera Elctrica "Alfredo C. Desages" (IIIE), and with the Departamento de Ingeniera Elctrica y de Computadoras of Universidad Nacional del Sur, Baha Blanca, Argentina, where he is a graduate Teaching Assistant.

Jorge A. Solsona (SM'04) received the Electronics Engineer and Dr. degrees from the Universidad Nacional de La Plata, La Plata, Argentina, in 1986 and 1995, respectively.

He is currently with the Departamento de Ingeniera Elctrica y de Computadoras, Instituto de Investigaciones en Ingeniera Elctrica "Alfredo C. Desages" (IIIE), Universidad Nacional del Sur, Baha Blanca, Argentina, where he is a Professor, and with CONICET. He is involved in teaching and research on control theory and its applications to electromechanical systems.